Determination of the moisture transport coefficient from pore network simulations of spontaneous imbibition in capillary porous media

Yasaman Jabbari[1], Evangelos Tsotsas[1], Christoph Kirsch[2], Abdolreza Kharaghani[1*]

[1] Thermal Process Engineering, Otto-von-Guericke University Magdeburg, Magdeburg, Germany

[2] Institute of Computational Physics, Zurich University of Applied Sciences, Winterthur, Switzerland

[*] Corresponding author. E-mail address: abdolreza.kharaghani@ovgu.de

Abstract

The Richards model for the spontaneous imbibition of a wetting liquid into a porous medium is revisited. Two methods are presented to determine the effective parameter in the Richards equation, i.e. the moisture transport coefficient D, from pore network simulations. In the first method, the capillary pressure and the relative permeability at different liquid saturations S, as well as the absolute permeability of the porous medium, are extracted using a quasi-static pore network model (QPNM) and then applied to estimate D(S). In contrast, in the second method, the function D is determined by an inverse method. The Richards equation is solved numerically with D(S) obtained from both methods and the solutions are compared to saturation levels over time achieved from a dynamic pore network model (DPNM), which is taken as a reference model in the present study. It is found that the solution of the Richards equation is very sensitive to the moisture transport coefficient D, especially when the porous medium is close to the fully saturated state. The saturation levels over time obtained from solving the Richards equation with D(S) calculated from the inverse method match well with those from the DPNM, whereas some discrepancy is observed when the QPNM is used to estimate D.

Keywords: Spontaneous imbibition, pore network models, Richards equation, parameter identification, scale transition

1. Introduction

The imbibition of a wetting phase into porous media is of great importance in the field of two-phase flow. This phenomenon plays an important role in various technical applications and scientific topics such as oil recovery (Standnes, 2004), paper coating (Ghassemzadeh and Sahimi, 2004), hygiene products (Sun et al., 2015) and agriculture (Lev and Blahovec, 2017). Imbibition can occur spontaneously or at a constant liquid flow rate. In the former case the capillary number ($Ca = \frac{\mu V}{\sigma}$, where μ, σ and V are the viscosity, surface tension and velocity of the wetting fluid, respectively) varies during the process whereas it is constant in the latter case. Furthermore, the imbibition can be quasi-static (very low liquid flow rate) or dynamic (large pressure drop along the medium) (Sahimi, 1995). Many methods have been proposed over the years specifically to study the kinetics of the imbibition processes as well as the evolution of the phase distribution as the wetting phase continues to displace the non-wetting phase. These studies include experimental works (Miranda et al., 2010; Roychaudhuri et al., 2013; Dai et al., 2017; David et al., 2017) and modeling approaches at different length scales such as molecular dynamics (Martic et al., 2002 ;Wang et al., 2017), lattice Boltzmann (Ahrenholz et al., 2008; Hatiboglu and Babadagli, 2008; Chapman et al., 2013; Arabjamaloei and Ruth, 2014), full morphology methods (Ashari and Vahedi Tafreshi, 2009; Zarandi and Pillai, 2018), pore network models (Thompson, 2002; Blunt et al., 2002; Tørå et al., 2012; Sun et al., 2016) and continuum models (Fries and Dreyer, 2008; Perez-Cruz et al., 2017; Deng and Wang, 2017).

A commonly used approach for the modeling of two-phase flow on the mesoscale is pore network modeling, which was first introduced by Fatt (1956). This method represents the void space of a porous medium as an interconnected network of pores and throats surrounded by the solid phase. The changes in the spatial distribution of the wetting and non-wetting fluids at each stage of the process are then determined by rules and events at the pore scale. Pore network models are divided into two classes: quasi-static (Thompson, 2002) and dynamic pore network models (Gruener et al., 2012). In the former, the only force determining the distribution of the phases is capillarity, whereas in the latter viscous forces also

contribute to the fluid motion. Pore network models may be used, among other applications, as a tool to characterize the porous medium and to extract single-phase and two-phase flow parameters.

Another widely surveyed simulation approach in the field of two-phase flow is continuum modeling. One of the well-known models for spontaneous imbibition is the Lucas-Washburn equation (Lucas, 1918;Washburn, 1921) which assumes a perfectly sharp imbibition front during the change of saturation. Neglecting inertial and gravitational forces, the Lucas-Washburn law states that the front height (distance between the wetting phase reservoir and the front) is directly proportional to the square root of time. Although the Lucas-Washburn equation has been widely used by scientists (Geromichalos et al., 2002; Gruener et al., 2012; Rieger et al., 2015), it fails to predict the phase distribution over time in several cases. Several attempts have been made to improve the model over the years (Bosanquet M.A., 1923; Fries and Dreyer, 2008; Cai and Yu, 2011).

In 1931, Richards proposed a continuum model for the fluid flow in unsaturated porous media (Richards, 1931). This model is derived from the conservation of mass together with Darcy's law (Darcy, 1856) as closure, and it has been employed in various scientific fields such as soil science (Witelski, 1997; Deng and Wang, 2017), characterization of paper (Perez-Cruz et al., 2017), fibrous materials (Zarandi and Pillai, 2018) etc. The Richards model is specifically beneficial under conditions without a sharp wetting front, e.g. in highly heterogeneous porous media for which the Lucas-Washburn law is not applicable. The Richards equation is mathematically a nonlinear diffusion equation; the effective parameter in this equation is the diffusion coefficient which needs to be determined a priori. This diffusion coefficient namely moisture transport coefficient (D), depends on a single-phase parameter, namely on the absolute permeability K_{abs} and on two two-phase parameters, namely the relative permeability K_r and the capillary pressure P_c.

One way to determine the effective parameters of the Richards model is to opt for experimental techniques such as the porous plate method, mercury injection, centrifuge method etc. (Purcell, 1949;

77 Sylte et al., 2004; Dernaika et al., 2012). These experimental methods provide a possibility to estimate
78 macroscopic parameters for real porous media rather than for simplified pore networks. Nevertheless, the
79 reduction of the experimental error, e.g. due to measurement devices, human error and environmental
80 conditions, is quite challenging.

81 Another widely used method to estimate the effective parameters of the Richards model is to utilize the
82 various empirical correlations which have been proposed over the decades (Burdine, 1953; Brooks and
83 Corey, 1964; van Genuchten, 1980; Landeryou et al., 2005). However, these correlations include other
84 unknown coefficients that need to be determined, e.g. by fitting. Furthermore, each of the empirical
85 equations is suitable only for specific systems and conditions and might not be applicable to other
86 situations. As mentioned, one of the applications of pore network models is in the estimation of single-
87 and multi-phase flow parameters. Jerauld and Salter (1990) developed a quasi-static pore network model
88 and used it to perform imbibition-drainage scanning loops. Blunt et al. (2002) determined relative
89 permeability curves in two- and three-phase systems by a quasi-static pore network model. Comparing
90 their results to experimental results from Oak (1990), they proved that pore network modeling is a
91 powerful tool to characterize multi-phase flow in porous media. Reeves and Celia (1996) proposed a
92 three-dimensional quasi-static pore network model capable of modeling both imbibition and drainage.
93 They concluded that a functional relationship between capillary pressure, liquid saturation and interfacial
94 area exists in two-phase flow. However, in all of these studies, the calculated parameters were not
95 employed in any continuum model to assess their usability for the prediction of the process kinetics.
96 Other authors derived the values of effective parameters from dynamic pore network modeling for
97 processes such as drainage (Joekar-Niasar et al., 2010), imbibition (Li et al., 2017) and drying (Attari
98 Moghaddam et al., 2017).

99 An alternative to the above-mentioned methods (which can be classified as “direct methods”) is an
100 “inverse method” to estimate the values of effective parameters. In an inverse method, we pursue the
101 backward path starting from kinetics data (i.e. liquid saturation as a function of time and space) and

proceeding towards effective parameters. By inverse modeling one can examine whether the physics of the process is well understood and whether the chosen model is consistent with the experimental conditions. Inverse methods have been previously utilized to estimate the effective parameters of two-phase flow processes (Gummerson et al., 1979;Pel et al., 1995;Ghaedi et al., 2015). However, they have not yet received enough attention by scientists for the calculation of the moisture transport coefficient, despite their promising potential due to the advanced optimization techniques which exist nowadays.

In this paper, the applicability of the Richards equation to predict the kinetics of spontaneous liquid imbibition into a porous medium is assessed. The (regular) structure of the pore network and the properties of the wetting and non-wetting fluids are described in Section 2.1, followed by a brief review of the dynamic pore network model (DPNM) in Section 2.2. In Section 2.3, two continuum models, namely the Lucas-Washburn law and the Richards equation are explained. In Section 2.4, the effective parameter of the Richards equation, i.e. the moisture transport coefficient D(S), is estimated using a quasi-static pore network model (QPNM) and an inverse method. In Section 3, the dependence of the moisture transport coefficient D on the liquid saturation S determined by different methods are presented and compared.. Furthermore, these D(S) curves are fed into the Richards equation and the numerical solutions are compared to the kinetic information predicted by the Lucas-Washburn law and by the DPNM, which is taken as a reference model in the present study. Finally, a summary of the methods as well as conclusions are presented in Section 4.

2. Methods

2.1. Model assumptions and pore network structure

The void space of the porous medium under study is a network of cylindrical throats interconnected via pores without volume in a regular grid. The throat radii are sampled from a monomodal normal distribution (Matlab's normrnd command) with given mean and standard deviation. For a real porous medium the pore size distribution can be characterized by measurement techniques such as mercury porosimetry, water retention method, photomicrographic methods, impregnation techniques, gas

adsorption method etc (Groen et al., 2003; Nimmo, 2004). Each pore in the network is connected to 6 throats having pre-determined equal lengths. The non-wetting and wetting fluids used here are air and water, respectively. The pressure drop in the gas phase is assumed to be negligible which is reasonable since the liquid has a much greater viscosity than the gas. Liquid flow in the throats is assumed to be laminar. The Reynolds number (Re) calculated by DPNM simulations goes into the laminar regime after 0.1 ms and the average Re number is 102.27. Moreover, inertial and gravitational forces are neglected. These assumptions can be assessed by calculating the dimensionless Weber (We) and Bond (Bo) numbers. The value of the Bo number, which shows the importance of the gravitational forces in comparison to the capillary forces is 0.0848 for our network. Since $Bo<<1$, gravitational forces are negligible. We number gives the ratio of inertial forces to capillary forces and (according to DPNM simulations) its average value drops below 1 already after 18 ms. Thus inertial forces are considered negligible. The process takes place under isothermal conditions and perfect wetting is assumed. The structural characteristics of the network as well as the physical properties of the fluids are listed in Table 1.

Liquid and gas reservoirs are placed at the bottom and top of the network, respectively. It is assumed that gas and liquid reservoirs are infinite i.e. they can provide unlimited amounts of gas and liquid, respectively. Initially, the network is filled with the gas phase. It is then brought into contact with the liquid reservoir, at which point spontaneous imbibition begins due to capillary forces. The displacement of the gas phase by the liquid phase continues until the network is fully saturated by liquid. The top boundary of the network is considered closed for liquid flow, i.e. no liquid invasion is possible through this boundary. However, the gas phase can escape through the top boundary and thereby leave the network. At the lateral boundaries, periodic boundary conditions are assumed. Figure 1 shows a small network with a liquid reservoir at its bottom.

Figure 1: Schematic representation of a small pore network (5×5×10 pores) connected to a liquid reservoir at the bottom.

Table 1: Properties of the network and of the fluids used in subsequent simulations.

2.2. Dynamic pore network model (DPNM)

In the dynamic pore network model (DPNM), both capillary and viscous forces influence the advancement of the liquid front. The network is initially filled with gas except for the pores adjacent to the liquid reservoir. Since there is no external force pumping the liquid into the network, these reservoir-connecting pores are at atmospheric pressure. Furthermore, the throats connected to these pores have a meniscus at their entrance. As the process starts, the following steps are taken in a consecutive manner:

- Pressure profile determination: Since laminar fluid flow is assumed, the volumetric liquid flow rate in a non-empty throat, q, is described by the Hagen-Poiseuille's equation:

$$q = \frac{\pi r^4}{8\mu L_w}(P_1 - P_2), \quad (1)$$

where L_w and r are the length of the liquid element in the throat and the throat radius, respectively. P_1 and P_2 are the pressure values at the two sides of the liquid element in the throat. For a saturated throat, these values are equal to the pressure values of the pores adjacent to this throat. However, if the throat is partially saturated and contains a meniscus, then the pressure of the liquid pore connected to the throat and the pressure at the liquid side of the meniscus are used as P_1 and P_2. The mass balance for any liquid pore that is not adjacent to the reservoir reads as

$$\sum_{i=1}^{n} q_i = 0, \quad (2)$$

where n is the number of throats connected to this liquid pore. In Eq.2, the only neighboring throats that are considered are full throats and partially saturated throats with a moving meniscus (invading or receding) at the side of the liquid pore. Collecting the mass balance equations for all liquid pores leads to a system of linear equations, the solution of which yields the pressure field throughout the network. It should be noted that this step is skipped when the network is in its initial state because

there is no liquid pore in the network except for the reservoir adjacent pore at the bottom of the network.

- Determination of the possible displacement events (invasion or retraction): When the pressure profile is known, stationary menisci (not moving), invading menisci (liquid filling the throat) and receding menisci (liquid leaving the throat) can be identified. In this model, it is possible to have multiple moving menisci at a specific time.
- Calculation of the time step size: The liquid flow rates in the throats containing moving (invading or retracting) menisci can be calculated by Eq.1. Among all displacement events, the one which first fills (in case of invasion) or empties (retraction) a throat is the decisive event. Therefore, the time step is defined as the time required for this meniscus to fill or empty the throat completely. All other invading or receding menisci will partially fill or empty the corresponding throats according to their flow rates and the time step size. At this stage, the values of L_w are updated based on the throat saturations from the previous time step and the displacement events which occurred during the current time step.
- Check for breakage: When a throat becomes empty, another pore-level event, called breakage, is possible. It occurs if the pressure in the connected liquid pore is not large enough to maintain the liquid continuity; as a result of breakage, a receding meniscus will form in one or more neighboring full throats.

After this step the current imbibition time is incremented by the calculated time step and the previous steps are repeated from the pressure calculation. The network saturation, local saturations (saturation at different heights of the network) and the current imbibition time are recorded at each time step. The process continues until the pore network is fully saturated. This model has been previously validated against experiments and is described in more detail in (Sun et al., 2016).

2.3. Continuum models

2.3.1. Lucas-Washburn law

The Lucas-Washburn law for a porous medium is derived from a momentum balance, assuming that the wetting front is perfectly flat and that the capillary pressure is constant during imbibition. Neglecting gravitational and inertial forces, the momentum balance for the system under study reads:

$$\frac{2\sigma\cos\theta}{r} = \frac{\varepsilon\mu h}{K_{abs}}\frac{dh}{dt}, \tag{3}$$

where h is the front height at time t and where θ is the equilibrium contact angle between liquid and gas. ε and K_{abs} are the porosity and absolute permeability of the network, respectively. The left-hand side of Eq. 3 denotes the capillary pressure calculated by the Young-Laplace equation and the right-hand side is the viscous pressure drop obtained by Darcy's law. Integration over time yields the Lucas-Washburn law for a porous medium:

$$h(t) = 2\sqrt{\frac{\sigma\cos\theta K_{abs}}{r\varepsilon\mu}}\sqrt{t}. \tag{4}$$

Assuming that the porosity is homogeneous in the network, the network saturation can be calculated as a function of time:

$$S_{net}(t) = \frac{h(t)}{H}, \tag{5}$$

where H is the total network height. Therefore:

$$S_{net}(t) = \frac{2}{H}\sqrt{\frac{\sigma\cos\theta K_{abs}}{r\varepsilon\mu}}\sqrt{t}. \tag{6}$$

Since the pore radii are distributed randomly in the network, we will take the mean value of the throat radii in Eq. 6.

2.3.2. Richards equation

For the one-dimensional (1D) spontaneous imbibition of a liquid into a gas-filled porous medium, the mass balance for the liquid phase reads:

$$\varepsilon \frac{\partial S}{\partial t} = -\frac{\partial u_s}{\partial z}, \tag{7}$$

where z and S are the vertical distance from the liquid reservoir and the local saturation, respectively. u_s is the superficial liquid velocity which appears in the generalized Darcy's law for two-phase flow:

$$u_s = -\frac{K_{abs} K_r}{\mu} \frac{\partial P_l}{\partial z}, \tag{8}$$

where P_l and K_r are the pressure and the relative permeability of the liquid phase, respectively. Assuming local capillary equilibrium, the liquid pressure and capillary pressure are linked via

$$P_l = P_g - P_c, \tag{9}$$

where P_g denotes the prescribed gas pressure. Combining Eqs. 7-9, the Richards equation is derived:

$$\varepsilon \frac{\partial S}{\partial t} = \frac{\partial}{\partial z}\left(-\frac{K_{abs} K_r(S)}{\mu} \frac{\partial P_c(S)}{\partial S} \frac{\partial S}{\partial z}\right). \tag{10}$$

Eq. 10 can be re-written in diffusion form:

$$\varepsilon \frac{\partial S}{\partial t} = \frac{\partial}{\partial z}\left(D(S) \frac{\partial S}{\partial z}\right). \tag{11}$$

where

$$D(S) = -\frac{K_{abs} K_r(S)}{\mu} \frac{\partial P_c(S)}{\partial S}, \tag{12}$$

is the moisture transport coefficient. Eq. 11 is solved together with the boundary conditions

$$S = 1 \text{ at } z = 0, \tag{13}$$

$$\frac{\partial S}{\partial z} = 0 \text{ at } z = H, \tag{14}$$

and with the initial condition

$$S = 0 \text{ at } t = 0. \tag{15}$$

2.4. Determination of the moisture transport coefficient

The determination of the effective parameters is a necessary step prior to the use of any continuum model. In the following sections two methods are introduced to estimate the effective parameter of the Richards equation, i.e. the moisture transport coefficient (Eq. 12). In the first method, we use the structural properties of the network together with a quasi-static pore network model (QPNM) as a simulation tool to estimate D(S); this method is referred to as a direct method. In contrast, the second method is an inverse method in which we use saturation profiles during the wetting process obtained from the DPNM to estimate D(S) via curve fitting.

2.4.1. Quasi-static pore network model (QPNM)

The pore network model presented in this section is based on the assumption that the viscous forces are negligible compared to the capillary forces (low Ca). This means that although the viscous forces still exist, their values are much smaller than the capillary forces so that the phase configuration at each overall saturation level is determined by the capillary forces only. When the viscous pressure drop is negligible, the gas and liquid phases retain the pressure of their respective reservoirs throughout the REV. Therefore, the capillary pressure, which is defined as the difference between the phase-averaged gas and liquid pressures, will be equal to the difference between the pressure in the gas and in the liquid reservoirs:

$$P_c = \langle P_g \rangle - \langle P_l \rangle = P_{g,R} - P_{l,R}, \tag{16}$$

where $\langle P_g \rangle$ and $\langle P_l \rangle$ are phase averaged pressures of gas and liquid. $P_{g,R}$ and $P_{g,R}$ denote the pressures in the gas and liquid reservoirs, respectively. The quasi-static imbibition is equivalent to an infinitely slow process where the system can be assumed in equilibrium at each stage. Since the Richards model assumes equilibrium in the local scale, the QPNM can be considered a suitable model to determine the moisture transport coefficient. This model is applied on a representative elementary volume (REV).

The REV is initially filled with the gas phase and the throats connected to the liquid reservoir at the bottom of the network contain menisci. These menisci are initially considered as stationary. This means that the contact angle of the meniscus is adjusted so that the liquid pressure behind the meniscus will be equal to the liquid pressure in the connected pore. The invasion mechanism is based on the invasion-percolation algorithm primarily proposed by Wilkinson and Willemsen (1983) and operates as follows:

1. The capillary thresholds of all throats are calculated by the Young-Laplace equation. For any throat i, the capillary threshold $P_{c,th,i}$ is given by:

$$P_{c,th,i} = \frac{2\sigma\cos\theta}{r_i}. \quad (17)$$

The pressure value calculated by Eq.17 is the pressure difference between gas and liquid phases when a moving meniscus exists in the throat. Having the capillary thresholds, the throat potential of each throat $\Phi_{th,i}$ can be calculated:

$$\Phi_{th,i} = P_g - P_{c,th,i}. \quad (18)$$

The throat potential indicates the liquid pressure behind the moving meniscus.

2. Liquid and gas reservoirs are set to constant pressures so that their difference i.e. the initial capillary pressure will be equal to the capillary threshold of the smallest throat (which has the largest capillary pressure by Eq.17) in the REV.
3. Each meniscus in the network is tested for stability. If the liquid pressure behind the meniscus (which is equal to the pressure of the liquid reservoir) is larger than the throat potential

$$P_{l,R} > \Phi_{th,i}, \quad (19)$$

the meniscus is marked as unstable. This is due to the fact that liquid always seeks a state with lower pressure (energy density). In other words, invasion is possible only if the liquid pressure behind the meniscus decreases by this displacement. Combining Eqs. 16 and 18 with the inequality19:

$$P_c < P_{c,th,i} \tag{20}$$

Hence, the capillary threshold of a throat can be understood as the maximum capillary pressure in which the liquid is allowed to flow into that throat.

4. In this model (as opposed to the DPNM), only one meniscus invades per step. From the menisci marked as "unstable", the smallest throat is chosen for invasion and its saturation changes from 0 to 1.
5. When a throat fills it will not contain a meniscus anymore and instead new menisci will be created at the entrance of all neighboring empty throats. The newly created menisci are considered stationary at this stage. The liquid pressure behind the meniscus is equal to the connected liquid pore and consequently to the pressure in the liquid reservoir.
6. The process is repeated from step 3 until there is no more unstable meniscus. This means that the system has reached equilibrium and no more liquid displacement is possible. At this stage, the values of capillary pressure and saturation are recorded.
7. The value of the capillary pressure (difference between gas and liquid reservoirs) is then decremented uniformly and the steps are repeated from 3.
8. The process continues until there is no more meniscus which means that the network is fully saturated.

To calculate the absolute permeability of the porous medium, we consider a fully saturated network. Under this condition the relative permeability is equal to unity (single-phase flow). A constant pressure difference ΔP is imposed across the network. Then, a similar method as in the DPNM (Eqs. 1-2) is applied to calculate the pressure profile. After this step, the total liquid flux across the network, Q, can be calculated by summing the liquid flow rates in a single layer of vertical throats. Using Darcy's law, K_{abs} is thus obtained as:

$$K_{abs} = \frac{Q\mu H_{REV}}{A_{REV}\Delta P}, \tag{21}$$

where A_{REV} and H_{REV} are the cross sectional area and the edge length of the REV, respectively.

The calculation of the relative permeability is fairly similar, except that the network must be partially saturated in this case. At each equilibrium stage of the QPNM, the liquid configuration is extracted and the corresponding pressure profile is calculated using Eqs. 1-2. Since equilibrium is assumed in the REV, the liquid flow rates through the individual layers of vertical throats are all identical and equal to the total flow rate. Thus, the total liquid flow rate Q passing the REV is determined by summing the flow rates in liquid-containing throats in any single layer of vertical throats. The generalized form of Darcy's law is utilized to calculate K_r for the respective saturation value:

$$K_r = \frac{Q\mu H_{REV}}{K_{abs} A_{REV} \Delta P}. \quad (22)$$

It should be noted that the calculation of K_r starts from the breakthrough saturation because before this stage no liquid is transferred through the network. Furthermore, only the spanning clusters, i.e. the liquid clusters which are connected to both the top and the bottom of the network, contribute to the liquid transport.

The combination of all three calculated parameters $P_c(S), K_{abs}$ and $K_r(S)$ leads to the moisture transport coefficient D(S) according to Eq. 12. These simulations are repeated 15 times for different network realizations and the obtained D(S) curves are averaged. For each realization, a new set of throat radii is generated randomly with the same values for the mean and standard deviation.

The calculated effective parameters should represent the full behavior of the intended structure and should thus be computed for a network size that includes all the structural properties. Therefore, the determination of the REV size is crucial. To do this, we run the QPNM on a cubic network with different sizes but with the same structural characteristics. We then compare the resulting capillary pressure curves and we search for the maximum size beyond which the curve does not change notably if the size is increased further. This is then taken as the size of the REV.

Empirical models: As mentioned, empirical equations are conventionally used in literature. Here, we choose empirical models for the capillary pressure and for the relative permeability and we fit them to the effective parameters calculated by the QPNM to assess the applicability of these models in predicting the wetting kinetics. For $P_c(S)$, the well-known van Genuchten correlation is adopted:

$$S_e = \frac{S - S_r}{1 - S_r} = \frac{1}{[1 + (\alpha P_c)^n]^m}, \tag{23}$$

and consequently:

$$\frac{dP_c(S)}{dS_e} = \frac{-1}{\alpha n m}\left(\left(\frac{1}{S_e}\right)^{\frac{1}{m}} - 1\right)^{\frac{1}{n}-1}\left(\frac{1}{S_e}\right)^{\frac{1}{m}+1}, \tag{24}$$

where S_e and S_r are the effective and residual liquid saturations, respectively. α and n are the fitting parameters, whereas $m = 1 - \frac{1}{n}$. Regarding $K_r(S)$, a power law is considered, as proposed by Brooks and Corey:

$$K_r = {S_e}^k, \tag{25}$$

where k is the fitting parameter. The fitting procedure is carried out in the software OriginPro 2017G.

Furthermore, considering the network as a bundle of parallel capillary tubes, the absolute permeability can be estimated as (Huinink, 2016):

$$K_{abs} = \frac{\varepsilon r^2}{8}. \tag{26}$$

However, in our pore network, only 1/3 of the throats are parallel to the z axis, i.e. the direction in which liquid is transported. Therefore the proper correlation for the absolute permeability in this case will be:

$$K_{abs} = \frac{\varepsilon r^2}{24}. \tag{27}$$

Therefore, we can build D based on empirical correlations, D_{Emp} by substituting Eqs. 24, 25 and 27 into Eq.12:

$$D_{Emp} = \frac{\varepsilon r^2}{24\mu\alpha nm} S_e{}^k \left(\left(\frac{1}{S_e}\right)^{\frac{1}{m}} - 1 \right)^{\frac{1}{n}-1} \left(\frac{1}{S_e}\right)^{\frac{1}{m}+1} \quad (28)$$

2.4.2. Inverse method

In this method, the kinetic data obtained from the DPNM is used to determine the moisture transport coefficient D(S). This is an inverse method since we use the behavior of the system during imbibition to establish the effective parameter D, rather than calculating this parameter from the geometrical structure of the network, as in Sec. 2.4.1.

The liquid saturations at each position in the network and at each time step are taken from the DPNM ($S_{DPNM}(t,z)$ at discrete points (t_i, z_i)). To estimate D(S), we first choose a specific number of points distributed equidistantly throughout the saturation range ($0 \leq S \leq 1$). Then, we attempt to find the best value of D corresponding to each of these points so that when the whole D(S) curve is fed into the Richards equation, the solution will have the least possible deviation to the results obtained from the DPNM. This deviation can be quantified by an objective function, E:

$$E = \sum_i \sum_j |S_{DPNM}(t_i, z_i) - S_{Richards}(t_i, z_i; D)|^2, \quad (29)$$

where $S_{Richards}$ is the solution of the Richards equation with the D(S) curve to be estimated. Eq. 29 implies that S_{DPNM} and $S_{Richards}$ match best (in the least-squares sense) when the value of E is minimal. This minimization problem can be handled by optimization techniques. In this work, the "patternsearch" function from Matlab's "Global optimization toolbox" is applied for this purpose. In order to achieve a smooth D(S) curve, a constraint is set for the problem to keep the total variation of D smaller than a prescribed absolute tolerance of 0.2.

3. Results and discussion

3.1. Liquid configuration and front width

The evolution of the wetting front during imbibition obtained from the DPNM is illustrated in Figure 2. The wetting front is rather sharp at the early stages of the process but it broadens as the network saturation increases. The reason is that, as the front height increases, the viscous force acts over a larger distance and thus the gradient of the pressure drop decreases. Therefore, the viscous forces become less pronounced compared to the capillary forces which leads to a more fractal-like front. Such a front broadening during spontaneous imbibition into a heterogeneous porous medium was reported previously (e.g. Dubé et al., 2000; Gruener et al., 2012; Chen et al., 2015). When the liquid reaches the top of the network through one of the surface throats, it can not invade further as the top boundary is impermeable for the liquid. Therefore, the imbibition front cannot advance further and its width eventually starts to decrease until the network is fully saturated. The front width, W, is quantified as:

$$W(t) = \sqrt{\langle (h_i(t) - \langle h_i(t) \rangle)^2 \rangle}, \tag{30}$$

where $h_i(t)$ is the height of meniscus i at time t. The operator $\langle \quad \rangle$ calculates the average of the intended expression over all menisci. Figure 3 shows the normalized front width against the network saturation. It can be seen that the front broadens until the breakthrough point. After this point, the width still increases a little further as the average front height $\langle h_i(t) \rangle$ is still increasing and the effect of the viscous pressure drop is more pronounced than the effect of the impermeable top boundary. Finally, at the last stages of the process, the front width decreases to zero.

From Figures 2 and 3, it can be concluded that a fairly large two-phase zone is observed during imbibition. Thus, the conventional Lucas-Washburn law could not predict the evolution of the front shape during imbibition properly as it is derived based on the assumption of the front being perfectly sharp.

Figure 2: Phase distributions during imbibition at different network saturations, S_{net}. (a) 0.1, (b) 0.5, (c) 0.9, (d) 1.

Figure 3: Normalized front width as a function of the network saturation.

3.2. Moisture transport coefficient

Figure 4 depicts P_c versus S obtained from the QPNM for pore networks with different sizes but with identical statistical characteristics. From this figure, it can be concluded that a cubic network with an edge length of 15 pores is large enough as the capillary pressure curve does not significantly change for larger sizes. Therefore, this size is chosen as the REV size.

Figures 5 and 6 show $P_c(S)$ and $K_r(S)$, respectively, calculated from running the QPNM simulation on the REV as well as from the corresponding fitted empirical correlations (Eqs. 23 and 25). It should be considered that the residual saturation S_r in Eq.23 is zero since the capillary pressure curve starts from zero saturation. Moreover, K_r obtained from QPNM in Figure 6 starts from the breakthrough saturation ($S_{\mathrm{Breakthrough}} = 0.0648$) as no liquid is transported through the REV below this saturation. The calculated fitting parameters and the goodness of fit are stated in Tables 2 and 3. The values of K_{abs} obtained from the QPNM and from Eq. 27 are presented in Table 4. From all of these parameters, D(S) can be calculated using Eq. 12.

Figure 7 demonstrates D(S) obtained from the QPNM, from empirical models, and from the inverse method. As can be seen, the curves from the QPNM and from the inverse method are quite close with only a slight difference near S = 1. The curve from the empirical models follows the same trend as the other two curves but it shows larger deviations especially at very high and very low saturations.

As observed from Figure 7, D determined from the QPNM has no value near S=0. This is due to the fact that one of the constituting parameters (K_r) can be calculated only after the breakthrough point. Similarly, the curve obtained from the inverse method starts from a nonzero saturation. The primary curve resulting from the optimization procedure (section 2.4.2) included out-of-range data points for small saturations

421 which were later omitted. It should also be noted that there are mathematical restrictions associated with
422 the utilized empirical correlations. In the van Genuchten equation (Eq. 23), P_c and consequently D_{Emp}
423 are undefined at S=0. Furthermore, $\frac{dP_c(S)}{dS}$ and D_{Emp} are not defined at S=1 according to Eqs. 20, 24 and
424 considering the values of fitting parameters (Table 3). It is however possible to calculate the limit of
425 D_{Emp} near S=1, where $\lim_{S\to 1^-} D_{Emp} = +\infty$. This can also be understood from the steep slope of the
426 capillary pressure curve (Figure 5) and the asymptotic behavior of the moisture transport coefficient curve
427 (Figure 7) as saturation approaches unity.

428 After the determination of the effective parameter D, the Richards equation is solved with D(S) obtained
429 from the QPNM and from the inverse method (Figure 7). For this, a finite volume method together with
430 the method of lines is used. The resulting solutions are then compared to the same results from the DPNM
431 which is taken as reference model.

432 Table 2: Fitting parameters of the van Genuchten equation for the capillary pressure and two measures for
433 the goodness of fit.

434 Table 3: Fitting parameters of the Brooks-Corey equation for the relative permeability and two measures
435 for the goodness of fit.

436 Table 4: Absolute permeability calculated from the QPNM and from a bundle of capillary model (Eq. 27)

437

438 Figure 4: Capillary pressure as a function of the liquid saturation for cubic networks with different edge
439 lengths obtained from the QPNM. The subplot depicts the capillary pressure curves at high saturation
440 values.

441 Figure 5: Capillary pressure as a function of the liquid saturation obtained from the QPNM and fitted
442 curve.

443 Figure 6: Relative permeability as a function of liquid saturation from the QPNM, and fitted curve.

444

Figure 7: Saturation-dependent moisture transport coefficient obtained from the QPNM, from the inverse method and from empirical models. The subplot depicts the curves in the range of high saturation values.

3.3. Evolution of the network saturation over time

The Richards equation is solved numerically with D(S) estimated from the QPNM and from the inverse method; we refer to these combinations as "QPNM-Richards" and "inverse method-Richards", respectively. The solution of the Richards equation yields the liquid saturation at different heights of the network during imbibition ($S(t,z)$) until the network is fully saturated. The total network saturation, S_{net} at each time can be calculated from the local saturation values:

$$S_{net}(t) = \frac{\sum_{i=1}^{N_e} V_{l,i}(t)}{\sum_{i=1}^{N_e} V_{v,i}} = \frac{\sum_{i=1}^{N_e} V_{v,i} S_i(t)}{\sum_{i=1}^{N_e} V_{v,i}}, \quad (31)$$

where V_l and V_v are the liquid and void volumes, respectively, of the discretized elements in the z-direction; and N_e is the number of these elements. Figure 8 illustrates the network saturation versus time obtained from QPNM-Richards, inverse method-Richards and from the Lucas-Washburn law. In this figure, the same quantities obtained by the reference method (DPNM), are also shown for comparison. As can be seen, the inverse method-Richards predicts a quite similar imbibition rate and total time as the DPNM. The figure also indicates that QPNM-Richards roughly estimates the imbibition rate and of the total imbibition time, however some deviation from the DPNM result is observed. This deviation is almost negligible at the beginning of the process but becomes more pronounced at later times. Moreover, it can be seen that the Lucas-Washburn law predicts a slightly faster imbibition compared to the DPNM. This can be justified through the connection between the front shape and the capillary number Ca. For a specific gas-liquid-solid system in a porous structure where the liquid invades with a sharp front, Ca is larger compared to the case where a wide and fractal-like front is observed. Considering the definition of Ca (Sec. 1) and the fact that the Lucas-Washburn law assumes a sharp front, it can be concluded that the Lucas-Washburn law is expected to predict a larger average liquid velocity than the DPNM.

Figure 8: Network saturation versus time obtained from the methods DPNM, QPNM-Richards, inverse method-Richards and from the Lucas-Washburn law.

3.4. Saturation profiles

The saturation profiles obtained from the three methods described in Sec. 2 are shown in Figure 9. ζ denotes the normalized position in the z direction. It can be seen that the curves obtained from the inverse method-Richards and from the DPNM are in good agreement. QPNM-Richards predicts similar results as the DPNM at early stages of the wetting process. However, as time proceeds, a discrepancy appears and QPNM-Richards predicts a slightly broader wetting front than the DPNM.

Figure 9: Saturation profiles at specific S_{net} values obtained from different methods. From left to right, S_{net} = 0.14, 0.24, 0.34, 0.44, 0.54, 0.64, 0.74, 0.84, 0.94.

3.5. Propagation of uncertainty

From the results presented herein, we observe that although the functions D(S) obtained from the estimation using the QPNM and the inverse method are similar (Figure 7) they lead to quite different predictions for the imbibition kinetics when used in the Richards equation (Figs. 8 and 9). This issue can be explained by the concept of uncertainty propagation. Any parameter estimation involves uncertainties of different types such as structural, algorithmic, interpolation and experimental uncertainties. In the case of determining D(S) by the QPNM, uncertainties can be introduced due to structural uncertainty, numerical errors (e.g. by calculating $\frac{dP_c}{dS}$ from P_c), assumptions underlying the employed model etc. One of the sources of (structural) uncertainty is the randomness of the pore sizes, which is quantifiable. For all realizations, the throat radii are sampled from a normal distribution with a prescribed mean and standard deviation. However, the throat radii are still random and the spatial distribution of small and large throats will be different for each realization, for example.

The uncertainty introduced in this way can be quantified by drawing a confidence band for the average

moisture transport coefficient ($D_{av}(S)$) considering D(S) from all realizations, ($D_i(S), i = 1,2, \dots 15$). Figure 10a depicts $D_{av}(S)$ and the corresponding 90% confidence band. As the figure indicates, the confidence band is very narrow which means that the level of uncertainty due to structural randomness of the REV is pretty low.

Figure 10: Propagation of uncertainty by the Richards equation. (a) Average moisture transport coefficient versus saturation obtained from the QPNM together with 90% confidence band and (b) the resulting network saturation versus time together with 90% confidence band.

If we insert all $D_i(S)$ curves and also $D_{av}(S)$ into the Richards equation and calculate the numerical solutions, then we can draw a confidence band for the network saturation S_{net} in a similar way. Figure 10b shows S_{net} obtained from using $D_{av}(S)$ into the Richards equation, $S_{net,av}$ against time and the corresponding 90% confidence band. Unlike in the estimation of D(S), the amount of uncertainty in the estimation of $S_{net}(t)$ appears to be high since the confidence band is quite wide. In other words, even though the uncertainty in the moisture transport coefficient is low, when it is fed into the Richards equation, the resulting network saturation will include a large level of uncertainty. This proves that the Richards equation is extremely sensitive to the coefficient function D(S) and that the uncertainty in the moisture transport coefficient is amplified over time when this equation is applied. Observing the propagation of uncertainty due to structural randomness (see Figure 10), one may expect that errors can also be introduced to D and thus to the imbibition kinetics from other sources, e.g. the numerical calculations.

This shows the importance of determining D with high precision as even small errors might lead to an inaccurate prediction of the imbibition rate and of the front width. This should be in fact considered while performing any direct method for the calculation of D(S). Considering this fact, it is expected that involving empirical correlations in the determination of D would lead to prediction of erroneous imbibition kinetics. The reason is that by applying empirical models for $P_c(S)$ (Eq. 23) and $K_r(S)$ (Eq. 25), a new source of uncertainty is introduced by the fitting procedure and the resulting D(S) will have a

lower level of accuracy. Furthermore, D determined by the adopted empirical correlations approaches infinity near S=1 which is unrealistic.

On the other hand, in the inverse method we adjust D(S) according to the discrepancy between the solutions S(t,z) of the Richards equation and of the DPNM. Therefore, if the value of the function E (Eq. 29) is small enough, it is assured that the obtained D(S) is the optimal curve which will lead to results close to those from the DPNM in the least-squares sense when it is fed into the Richards equation. However, to implement an inverse method we need to know $S(t, z)$ as primary information. This requires time- consuming experimental measurements or dynamic numerical simulations which are normally computationally expensive. In contrast, the QPNM is a high-speed tool which is able to estimate D(S) with a reasonable precision if a proper averaging procedure is employed.

4. Conclusions

In this study, the Richards equation is revisited and its capability to predict the process kinetics during the spontaneous imbibition of a liquid into a gas-filled porous medium with an effective moisture transport coefficient calculated from different methods is assessed. A direct method using a quasi-static pore network model (QPNM) and an inverse method using a dynamic pore network model (DPNM) are developed to estimate the moisture transport coefficient from numerical simulations. The functions D(S) obtained by these two methods are quite similar except near S = 1. Moreover, conventional empirical equations (van Genuchten and Brooks-Corey for $P_c(S)$ and $K_r(S)$, respectively) are fitted to curves calculated from the QPNM and are then employed to determine D. Although good fits are obtained, the resulting D(S) shows a discrepancy to the other two curves (Figure 7), especially at very high and at very low saturations.

The Richards equation is then solved numerically for the different calculated D(S) curves using the finite volume method and the numerical solutions of the Richards equation are compared to the results obtained from the dynamic pore network model (DPNM) (Figs. 8, 9). A good agreement was achieved between the

saturation levels $S(t,z)$ predicted by the inverse method-Richards approach and by the DPNM. This proves that the inverse method estimates D(S) well and the value of the objective function E is small enough. The QPNM-Richards approach represents satisfying results with some deviation compared to the DPNM, despite the fact that D(S) computed from the QPNM and from the inverse method are very close. The reason is the high sensitivity of the Richards equation to the moisture transport coefficient function. From the average D(S) calculated from the QPNM, the resulting network saturation curve and their corresponding confidence bands, it is quite obvious that the uncertainty in the determined effective parameter D is amplified strongly over time when it is fed into the Richards equation. Thus, it can be predicted that if one applies empirical models for the determination of P_c and K_r and uses the resulting D as an input for the Richards equation, then the obtained imbibition kinetics will be erroneous and unrealistic. When a fitting step is involved in the determination of D(S), an extra source of uncertainty is added which will propagate into the solution of the Richards equation. Thus, although the use of these empirical correlations gives smooth curves for the effective parameters, it might lead to an inaccurate prediction of the imbibition rate and of the wetting front width. Furthermore, comparing the values of the network saturation during imbibition calculated by the DPNM and by the Lucas-Washburn law (Figure 8) confirms that, although the Lucas-Washburn law is not able to predict the front shape properly, it estimates the evolution of the total network saturation over time with a reasonably small error. Finally, our results show that none of the continuum models used here can reproduce precisely the same S(t,z) as obtained from our (discrete) DPNM.

On the one hand, to estimate D(S) from an inverse method, we used the saturation profiles $S(t,z)$ during the wetting process obtained from the DPNM (which is a time-consuming and computationally expensive model) as inputs. The QPNM, on the other hand, is fast and efficient since only capillary thresholds of the throats need to be considered to determine the phase saturation at each step. Furthermore, to characterize the structure of the medium, the QPNM is applied to a network with an REV size of $15 \times 15 \times 15$ pores, which is one quarter of the size of the main network under study ($15 \times 15 \times 60$ pores).

In conclusion, for engineering purposes, where a rough estimation of the behavior of the system is needed, the QPNM is an efficient tool. However, in theoretical work where the determination of D(S) with high precision is crucial it is safer to use the inverse method.

It should be considered that gravitational forces are neglected in the current study which is valid under specific conditions, e.g. for horizontal liquid transport. However, the continuum model and the DPNM can be extended in a future study to account for the gravitational forces to test the methods also for cases in which gravity plays an important role. Moreover, the pore network models can be improved in order to include the contact angle hysteresis effect or to become suitable for more complex network structures such as irregular pore shape, tortuous throats, non-uniform coordination number of pores etc. In addition, the proposed methods can be utilized to build a correlation between D(S) and the structural properties of the medium such as the pore size distribution, the coordination number of pores, the pore geometry, etc.

Acknowledgments

This work was financially supported by the German Research Foundation (DFG) within the framework of the Graduate School 1554 “Micro-Macro-Interactions in Structured Media and Particulate Systems”. The authors are grateful to the anonymous reviewers for their constructive comments.

References

Ahrenholz, B., Tölke, J., Lehmann, P., Peters, A., Kaestner, A., Krafczyk, M., Durner, W., 2008. Prediction of capillary hysteresis in a porous material using lattice-Boltzmann methods and comparison to experimental data and a morphological pore network model. Adv. Water Resour. 31, 1151–1173. https://doi.org/10.1016/j.advwatres.2008.03.009

Arabjamaloei, R., Ruth, D., 2014. Simulation of counter-current spontaneous imbibition in a simple porous medium using Lattice-Boltzmann, in: International Symposium of the Society of Core Analysts. p. 62.

589 Ashari, A., Vahedi Tafreshi, H., 2009. A two-scale modeling of motion-induced fluid release from thin
590 fibrous porous media. Chem. Eng. Sci. 64, 2067–2075. https://doi.org/10.1016/j.ces.2009.01.048

591 Attari Moghaddam, A., Prat, M., Tsotsas, E., Kharaghani, A., 2017. Evaporation in capillary porous
592 media at the perfect piston-like invasion limit: Evidence of nonlocal equilibrium effects. Water
593 Resour. Res. 53, 10433–10449. https://doi.org/10.1002/2017WR021162

594 Blunt, M.J., Jackson, M.D., Piri, M., Valvatne, P.H., 2002. Detailed physics, predictive capabilities and
595 macroscopic consequences for pore-network models of multiphase flow. Adv. Water Resour. 25,
596 1069–1089. https://doi.org/10.1016/S0309-1708(02)00049-0

597 Bosanquet M.A, C.H., 1923. On the flow of liquids into capillary tubes. London, Edinburgh, Dublin
598 Philos. Mag. J. Sci. 45, 525–531. https://doi.org/10.1080/14786442308634144

599 Brooks, R.H., Corey, A.T., 1964. Hydraulic properties of porous media. Hydrol. Pap. 3.
600 https://doi.org/citeulike-article-id:711012

601 Burdine, N.T., 1953. Relative permeability calculations from pore size distribution data. J. Pet. Technol.
602 198, 71–78. https://doi.org/10.2118/225-G

603 Cai, J., Yu, B., 2011. A discussion of the effect of tortuosity on the capillary imbibition in porous media.
604 Transp. Porous Media 89, 251–263. https://doi.org/10.1007/s11242-011-9767-0

605 Chapman, E.M., Yang, J., Crawshaw, J.P., Boek, E.S., 2013. Pore scale models for imbibition of
606 CO2analogue fluids in etched micro-fluidic junctions from micro-model experiments and direct
607 LBM flow calculations. Energy Procedia 37, 3680–3686.
608 https://doi.org/10.1016/j.egypro.2013.06.262

609 Chen, Y.J., Watanabe, S., Yoshikawa, K., 2015. Roughening dynamics of radial imbibition in a porous
610 medium. J. Phys. Chem. C 119, 12508–12513. https://doi.org/10.1021/acs.jpcc.5b03157

611 Dai, C., Wang, X., Li, Y., Lv, W., Zou, C., Gao, M., Zhao, M., 2017. Spontaneous imbibition
612 investigation of self-dispersing silica nanofluids for enhanced oil recovery in low-permeability
613 cores. Energy and Fuels 31, 2663–2668. https://doi.org/10.1021/acs.energyfuels.6b03244

614 Darcy, H., 1856. Les fontaines publiques de la ville de Dijon : exposition et application des principes à
615 suivre et des formules à employer dans les questions de distribution d'eau. Recherche 647.
616 https://doi.org/10.2516/ogst

617 David, C., Sarout, J., Dautriat, J., Pimienta, L., Michée, M., Desrues, M., Barnes, C., 2017. Ultrasonic
618 monitoring of spontaneous imbibition experiments: Precursory moisture diffusion effects ahead of
619 water front. J. Geophys. Res. Solid Earth 122, 4948–4962. https://doi.org/10.1002/2017JB014193

620 Deng, B., Wang, J., 2017. Saturated-unsaturated groundwater modeling using 3D Richards equation with
621 a coordinate transform of nonorthogonal grids. Appl. Math. Model. 50, 39–52.
622 https://doi.org/10.1016/j.apm.2017.05.021

623 Dernaika, M.R., Kalam, M.Z., Basioni, M., Dawoud, A., Skjæveland, S.M., 2012. Hysteresis of capillary
624 pressure, resistivity index and relative permeability in different carbonate rock types, in: Society of
625 Petrophysicists and Well-Log Analysts.

626 Dubé, M., Rost, M., Alava, M., 2000. Conserved dynamics and interface roughening in spontaneous
627 imbibition : A critical overview. Eur. Phys. J. B 15, 691–699.

628 Zarandi, M.A.F., Pillai, K.M., 2018. Spontaneous imbibition of liquid in glass fiber wicks, Part II:
629 Validation of a diffuse-front model. AIChE J. 64, 306–315. https://doi.org/10.1002/aic.15856

630 Fatt, I., 1956. The network model of porous media. Pet. Trans. AIME 207, 144–181.

631 Fries, N., Dreyer, M., 2008. An analytic solution of capillary rise restrained by gravity. J. Colloid
632 Interface Sci. 320, 259–263. https://doi.org/10.1016/j.jcis.2008.01.009

633 Geromichalos, D., Mugele, F., Herminghaus, S., 2002. Nonlocal dynamics of spontaneous imbibition
634 fronts. Phys. Rev. Lett. 89. https://doi.org/10.1103/PhysRevLett.89.104503

635 Ghaedi, M., Heinemann, Z.E., Masihi, M., Ghazanfari, M.H., 2015. An efficient method for determining
636 capillary pressure and relative permeability curves from spontaneous imbibition data. Iran. J. Oil
637 Gas Sci. Technol. 4, 1–17. https://doi.org/10.22050/ijogst.2015.10364

638 Ghassemzadeh, J., Sahimi, M., 2004. Pore network simulation of fluid imbibition into paper during
639 coating - III: Modelling of the two-phase flow. Chem. Eng. Sci. 59, 2281–2296.
640 https://doi.org/10.1016/j.ces.2004.01.058

641 Groen, J.C., Peffer, L.A.A., Perez-Ramirez, J., 2003. Pore size determination in modified micro- and
642 mesoporous materials . Pitfalls and limitations in gas adsorption data analysis 60, 1–17.
643 https://doi.org/10.1016/S1387-1811(03)00339-1

644 Gruener, S., Sadjadi, Z., Hermes, H.E., Kityk, A. V., Knorr, K., Egelhaaf, S.U., Rieger, H., Huber, P.,
645 2012. Anomalous front broadening during spontaneous imbibition in a matrix with elongated pores.
646 Proc. Natl. Acad. Sci. 109, 10245–10250. https://doi.org/10.1073/pnas.1119352109

647 Gummerson, R.J., Hall, C., Hoff, W.D., Hawkes, R., Holland, G.N., Moore, W.S., 1979. Unsaturated
648 water flow within porous materials observed by NMR imaging. Nature 281, 56–57.

649 Hatiboglu, C.U., Babadagli, T., 2008. Pore-scale studies of spontaneous imbibition into oil-saturated
650 porous media. Phys. Rev. E - Stat. Nonlinear, Soft Matter Phys. 77, 066311.
651 https://doi.org/10.1103/PhysRevE.77.066311

652 Huinink, H., 2016. Fluids in porous media transport and phase changes. Morgan & Claypool Publishers,
653 San Rafael.

654 Jerauld, G.R., Salter, S.J., 1990. The effect of pore-structure on hysteresis in relative permeability and

capillary pressure: Pore level modeling. Transp. Porous Media 5, 103–151.

Joekar-Niasar, V., Hassanizadeh, S.M., Dahle, H.K., 2010. Non-equilibrium effects in capillarity and interfacial area in two-phase flow: Dynamic pore-network modelling. J. Fluid Mech. 655, 38–71. https://doi.org/10.1017/S0022112010000704

Landeryou, M., Eames, I., Cottenden, A., 2005. Infiltration into inclined fibrous sheets. J. Fluid Mech. 529, 173–193. https://doi.org/10.1017/S0022112005003356

Lev, J., Blahovec, J., 2017. Imbibition of wheat seeds: Application of image analysis. Int. Agrophysics 31, 475–481. https://doi.org/10.1515/intag-2016-0072

Li, J., McDougall, S.R., Sorbie, K.S., 2017. Dynamic pore-scale network model (PNM) of water imbibition in porous media. Adv. Water Resour. 107, 191–211. https://doi.org/10.1016/j.advwatres.2017.06.017

Lucas, R., 1918. On the time law of the capillary rise of liquids. Kolloid-Zeitschrift 23, 15–22. https://doi.org/10.1007/BF01461107

Martic, G., Gentner, F., Seveno, D., Coulon, D., De Coninck, J., Blake, T.D., 2002. A molecular dynamics simulation of capillary imbibition. Langmuir 18, 7971–7976. https://doi.org/10.1021/la020068n

Miranda, A.M., Menezes-Sobrinho, I.L., Couto, M.S., 2010. Spontaneous imbibition experiment in newspaper sheets. Phys. Rev. Lett. 104, 086101. https://doi.org/10.1103/PhysRevLett.104.086101

Nimmo, J.R., 2004. Porosity and Pore Size Distribution, Hillel, D., ed. Encyclopedia of Soils in the Environment.

Oak, M.J., 1990. Three-phase relative permeability of water-wet berea, in: Paper SPE 20183, Proceedings of the SPE/DOE Seventh Symposium on Enhanced Oil Recovery. Tulsa, Oklahoma.

677 Pel, L., Kopinga, K., Bertram, G., Lang, G., 1995. Water absorption in a fired-clay brick observed by
678 NMR scanning. J. Phys. D. Appl. Phys. 28, 675–680. https://doi.org/10.1088/0022-3727/28/4/009

679 Perez-Cruz, A., Stiharu, I., Dominguez-Gonzalez, A., 2017. Two-dimensional model of imbibition into
680 paper-based networks using Richards' equation. Microfluid. Nanofluidics 21, 98.
681 https://doi.org/10.1007/s10404-017-1937-0

682 Purcell, W.R., 1949. Capillary pressures -their measurement using mercury and the calculation of
683 permeability therefrom. J. Pet. Technol. 1, 39–48. https://doi.org/10.2118/949039-G

684 Reeves, P.C., Celia, M.A., 1996. A functional-relationship between capillary-pressure, saturation, and
685 interfacial area as revealed by a pore-scale network model. Water Resour. Res. 32, 2345–2358.
686 https://doi.org/10.1029/96WR01105

687 Richards, L.A., 1931. Capillary conduction of liquids through porous mediums. Physics (College. Park.
688 Md). 1, 318–333.

689 Rieger, H., Thome, C., Sadjadi, Z., 2015. Meniscus arrest dominated imbibition front roughening in
690 porous media with elongated pores. J. Phys. Conf. Ser. 638. https://doi.org/10.1088/1742-
691 6596/638/1/012007

692 Roychaudhuri, B., Tsotsis, T.T., Jessen, K., 2013. An experimental investigation of spontaneous
693 imbibition in gas shales. J. Pet. Sci. Eng. 111, 87–97. https://doi.org/10.1016/j.petrol.2013.10.002

694 Sahimi, M., 1995. Flow and transport in porous media and fractured rock: From classical methods to
695 modern approaches. VCH, Weinheim.

696 Standnes, D.C., 2004. Analysis of oil recovery rates for spontaneous imbibition of aqueous surfactant
697 solutions into preferential oil-wet carbonates by estimation of capillary diffusivity coefficients.
698 Colloids Surfaces A Physicochem. Eng. Asp. 251, 93–101.

https://doi.org/10.1016/j.colsurfa.2004.09.013

Sun, Y., Kharaghani, A., Metzger, T., Müller, J., Tsotsas, E., 2015. Lotion distribution in wet wipes investigated by pore network simulation and X-ray micro tomography. Transp. Porous Media 107, 449–468. https://doi.org/10.1007/s11242-014-0448-7

Sun, Y., Kharaghani, A., Tsotsas, E., 2016. Micro-model experiments and pore network simulations of liquid imbibition in porous media. Chem. Eng. Sci. 150, 41–53. https://doi.org/10.1016/j.ces.2016.04.055

Sylte, A., Ebeltoft, E., Petersen, E.B., 2004. Simultaneous determination of relative permeability and capillary pressure using data from several experiments, in: International Symposium of the Society of Core Analysts.

Thompson, K.E., 2002. Pore-scale modeling of fluid transport in disordered fibrous materials. AIChE J. 48, 1369–1389. https://doi.org/10.1002/aic.690480703

Tørå, G., Øren, P.E., Hansen, A., 2012. A dynamic network model for two-phase flow in porous media. Transp. Porous Media 92, 145–164. https://doi.org/10.1007/s11242-011-9895-6

van Genuchten, M.T., 1980. A closed-form equation for predicting the hydraulic conductivity of unsaturated soils. Soil Sci. Soc. Am. J. 44, 892–898. https://doi.org/10.2136/sssaj1980.03615995004400050002x

Wang, X., Xiao, S., Zhang, Z., He, J., 2017. Effect of nanoparticles on spontaneous imbibition of water into ultraconfined reservoir capillary by molecular dynamics simulation. Energies 10, 506. https://doi.org/10.3390/en10040506

Washburn, E.W., 1921. The dynamics of capillary flow. Phys. Rev. 17, 273–283. https://doi.org/10.1103/PhysRev.17.273

721 Wilkinson, D., Willemsen, J.F., 1983. Invasion percolation: A new form of percolation theory. J. Phys. A.
722 Math. Gen. 16, 3365–3376. https://doi.org/10.1088/0305-4470/16/14/028

723 Witelski, T.P., 1997. Perturbation analysis for wetting fronts in Richard's equation. Transp. Porous Media
724 27, 121–134.

Figure 1

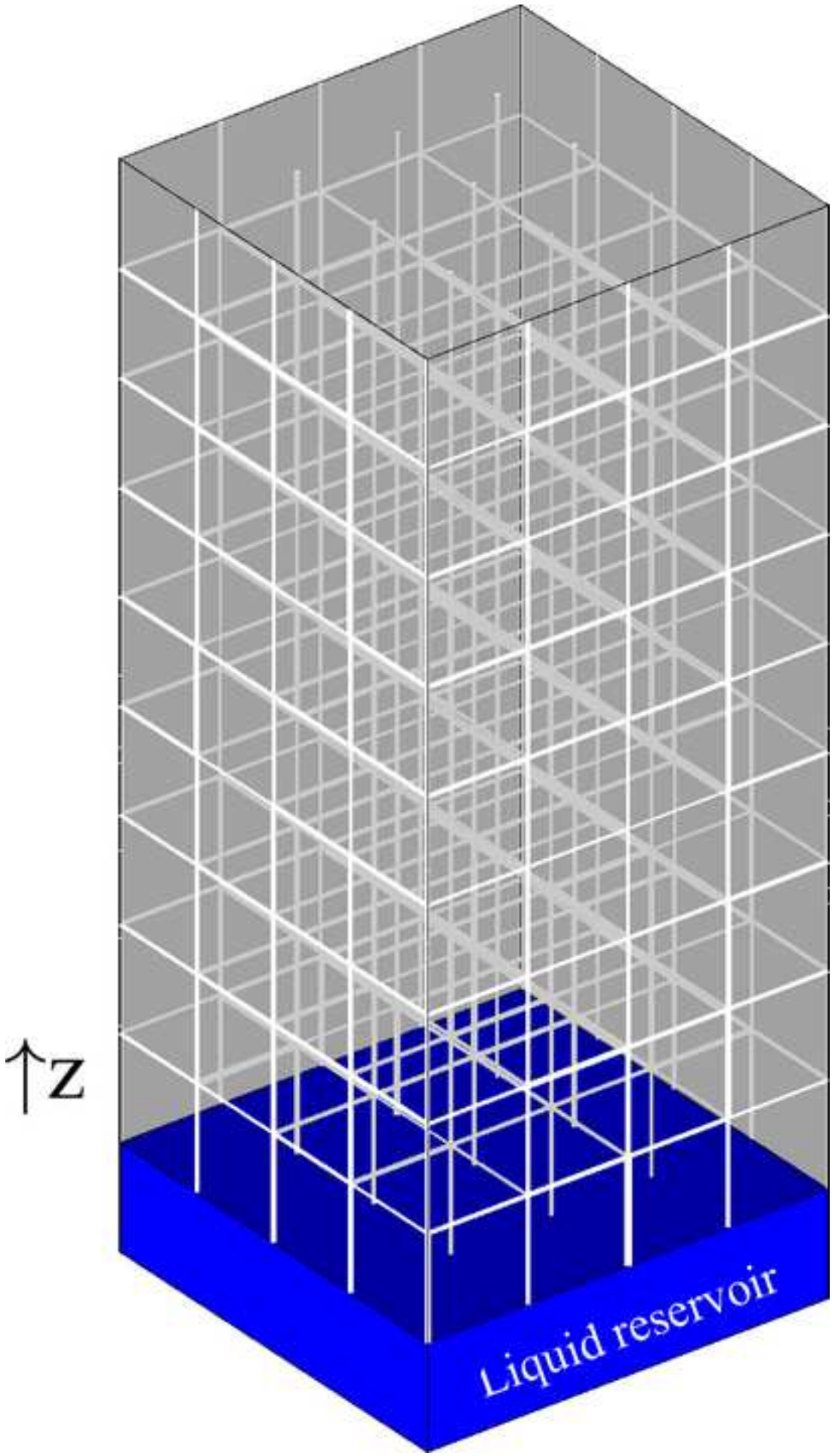

Figure 2a

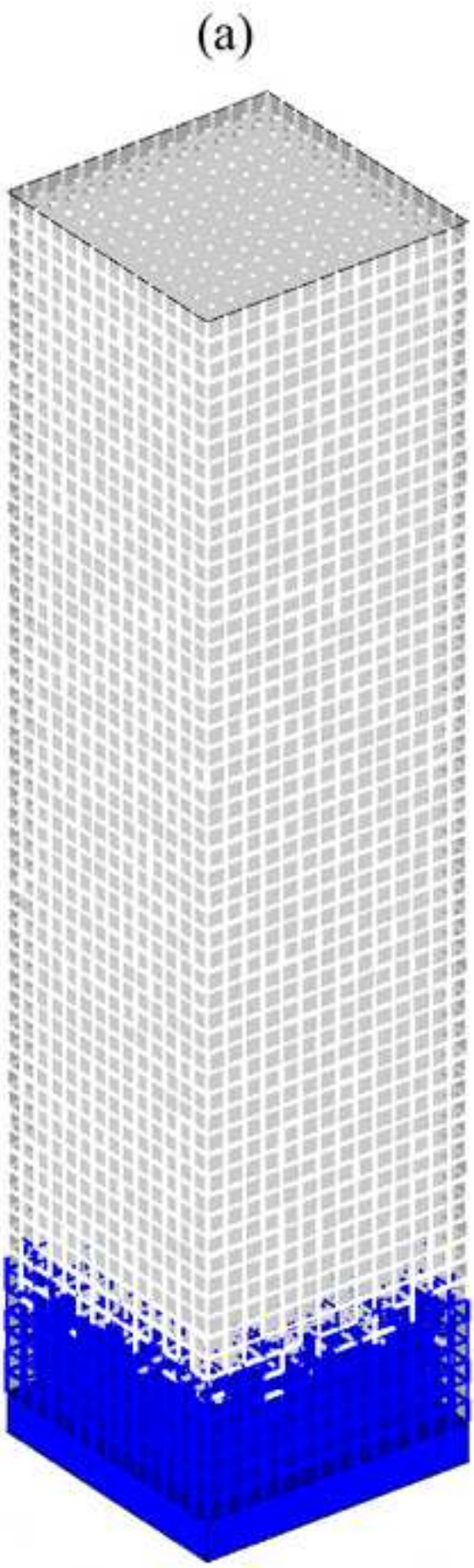

Figure 2b

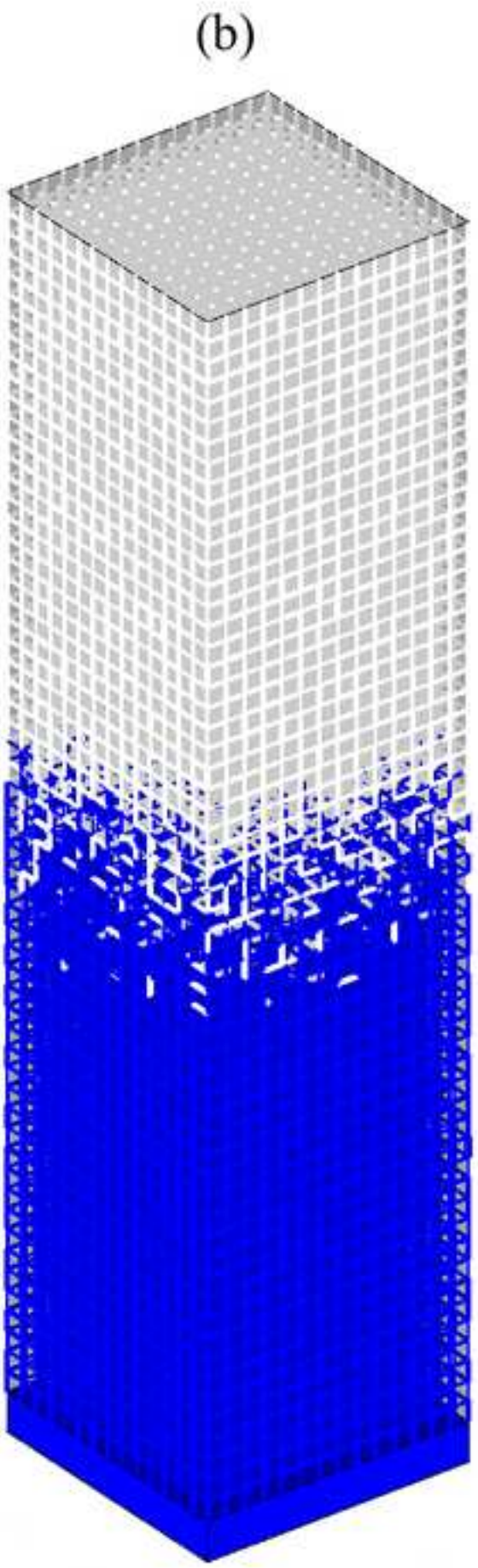

Figure 2c

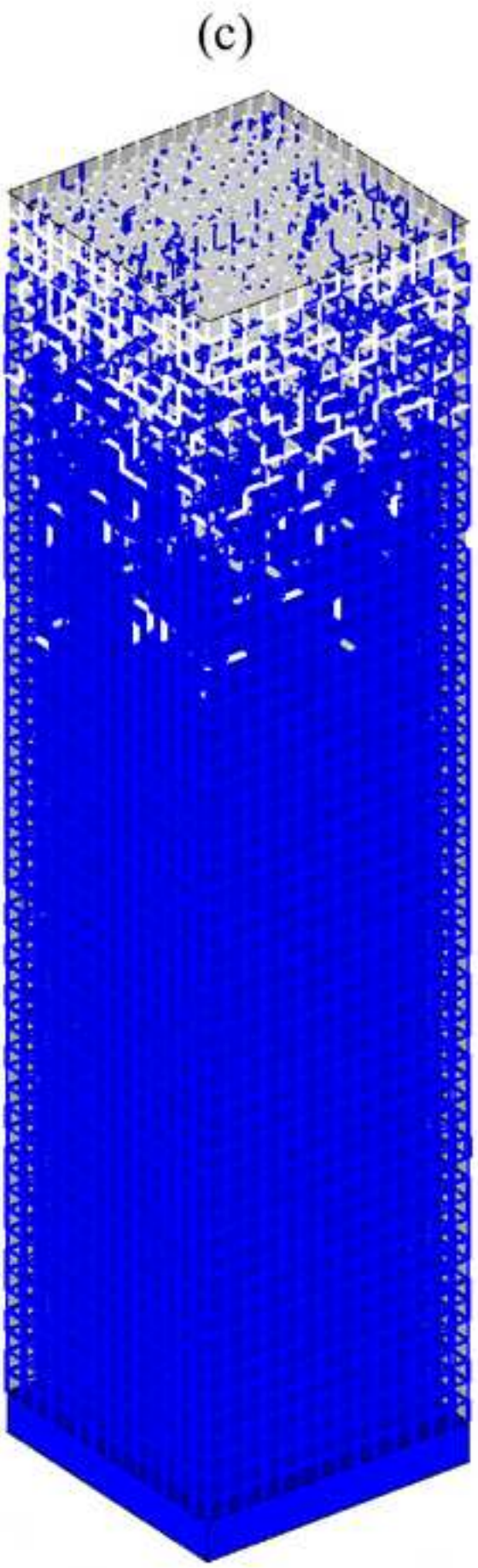

Figure 2d

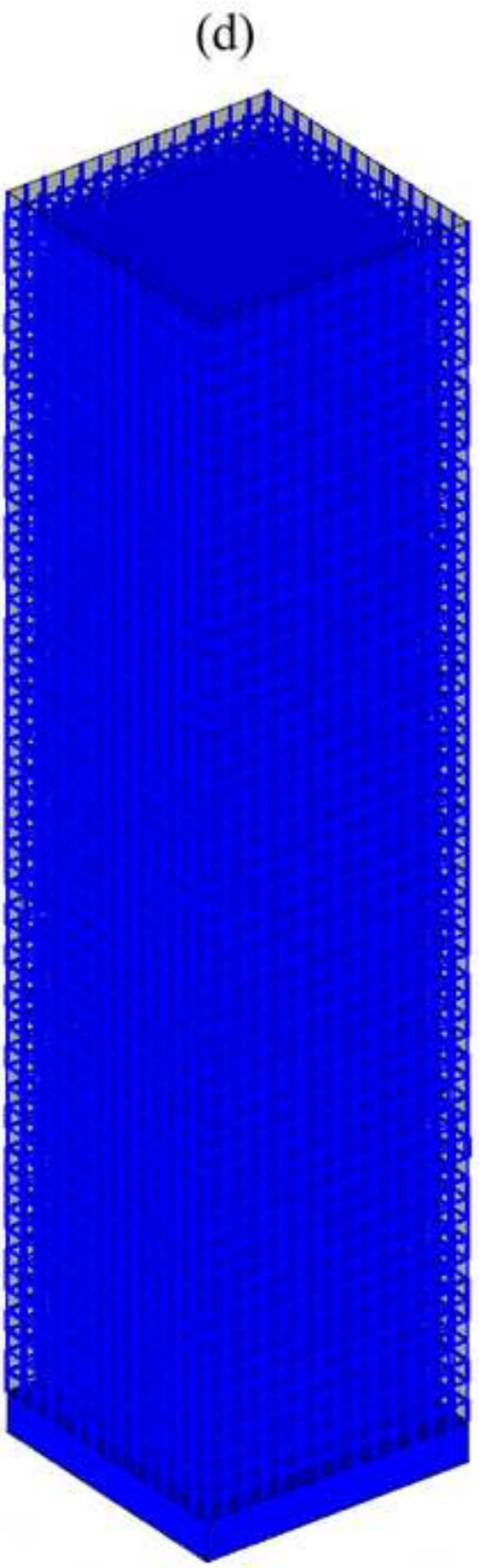

Figure 3

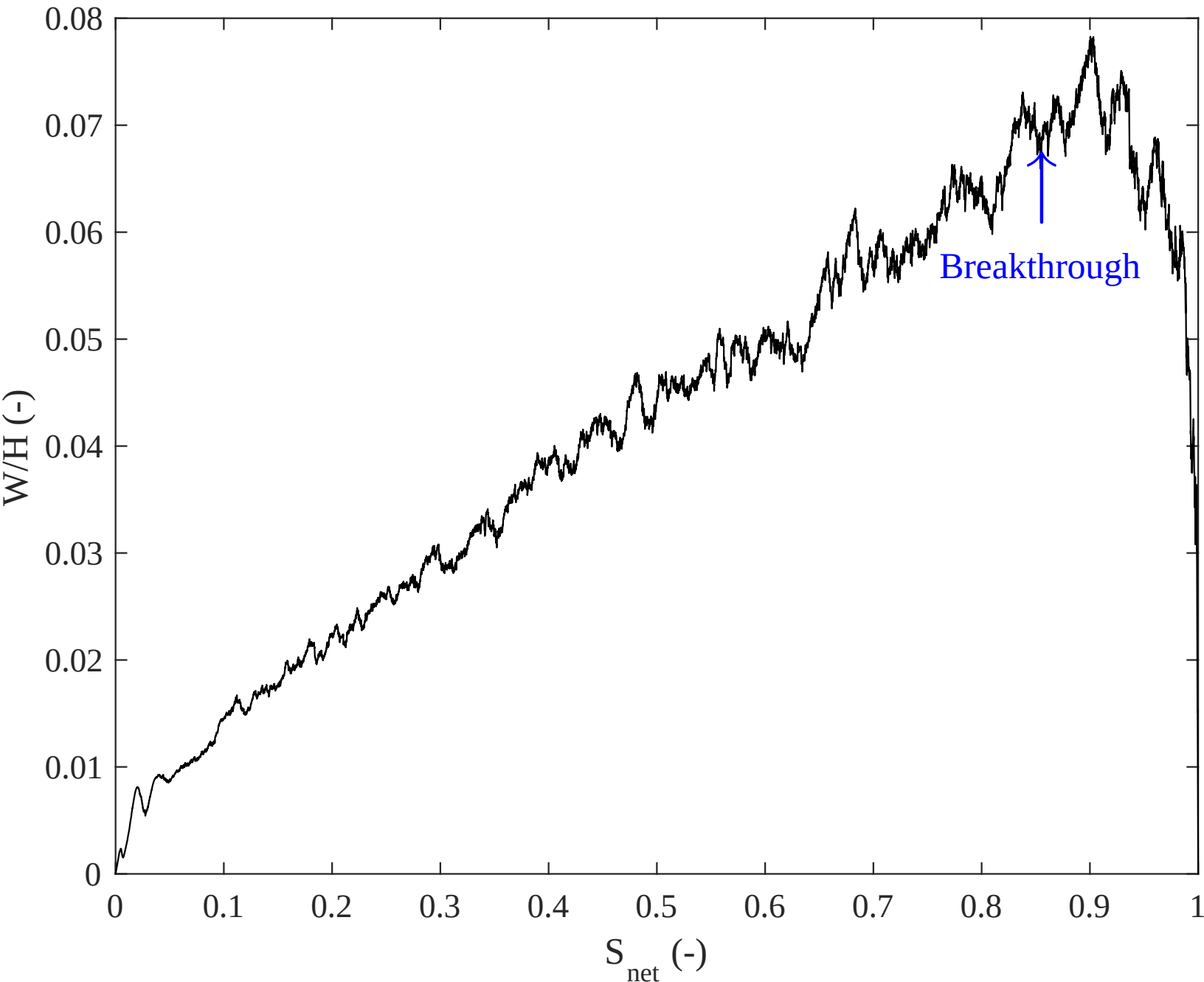
0.08
0.07
0.06
0.05
0.04
0.03
0.02
0.01
0
W/H (-)
0
0.1
0.2
0.3
0.4
0.5
0.6
0.7
0.8
0.9
1
S net (-)
Breakthrough

Figure 4

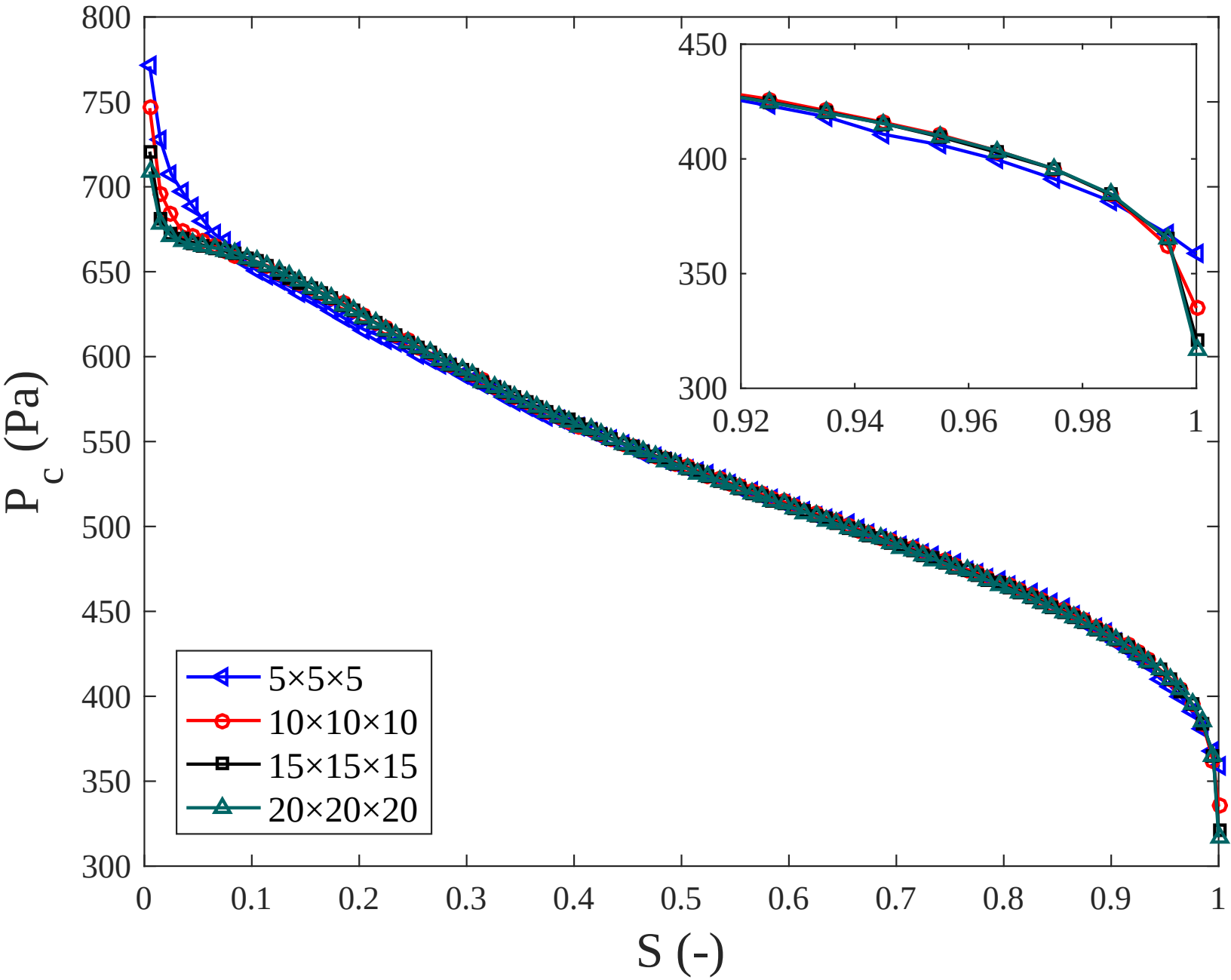
800
750
700
650
600
550
500
450
400
350
300
P c (Pa)
0
0.1
0.2
0.3
0.4
0.5
0.6
0.7
0.8
0.9
1
S (-)
5×5×5
10×10×10
15×15×15
20×20×20
450
400
350
300
0.92
0.94
0.96
0.98
1

Figure 5

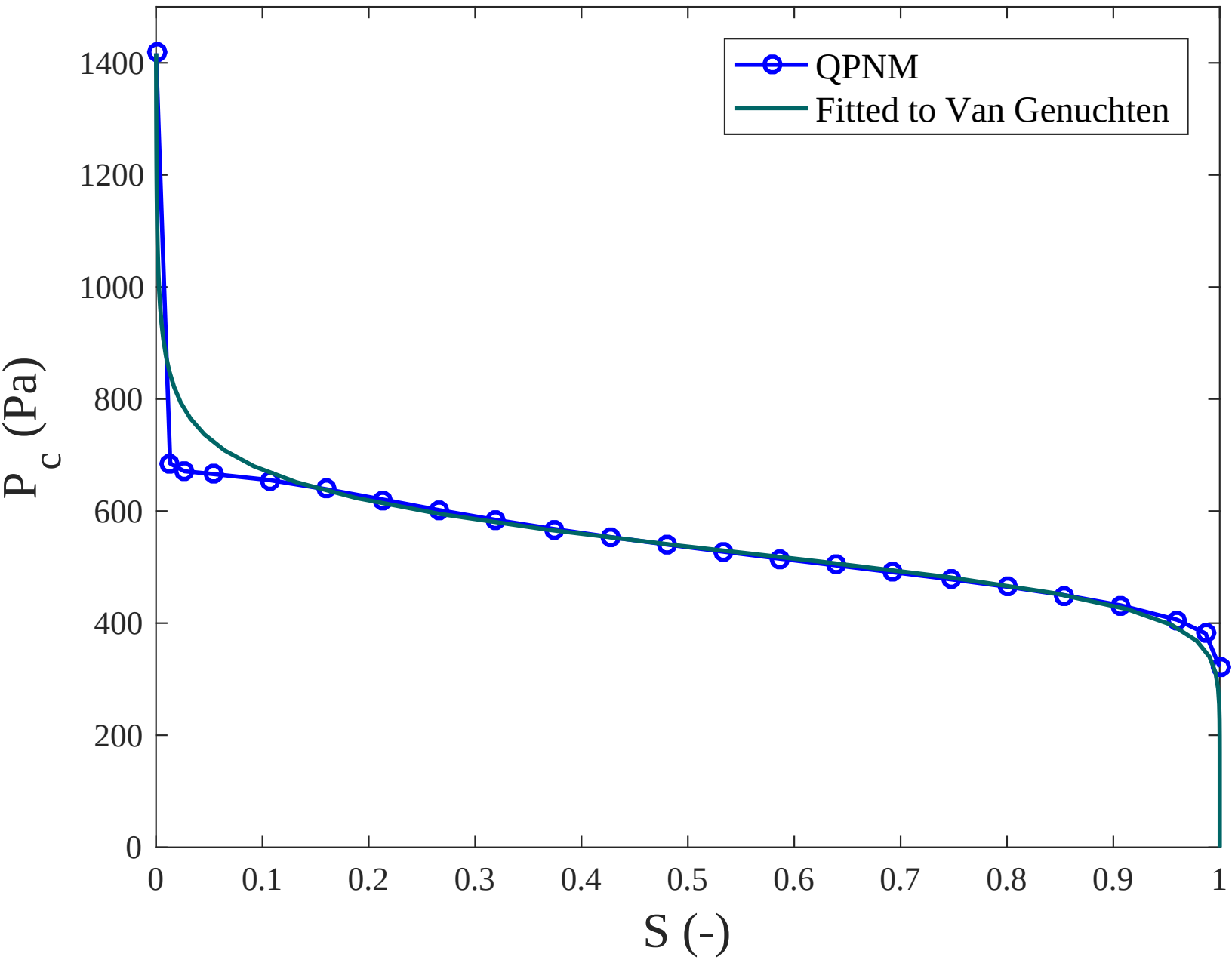
QPNM
Fitted to Van Genuchten
P c (Pa)
S (-)
0
200
400
600
800
1000
1200
1400
0
0.1
0.2
0.3
0.4
0.5
0.6
0.7
0.8
0.9
1

Figure 6

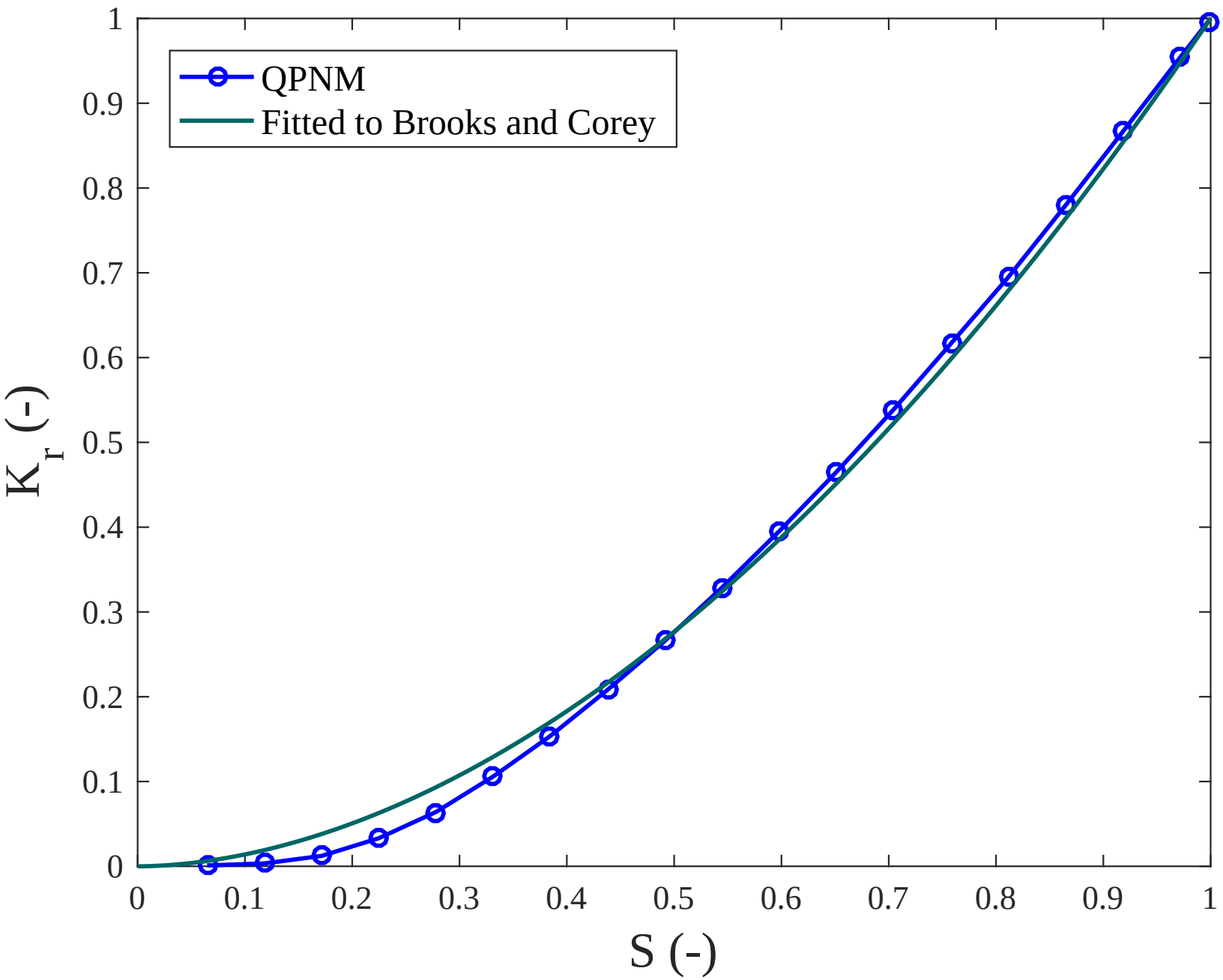

Figure 7

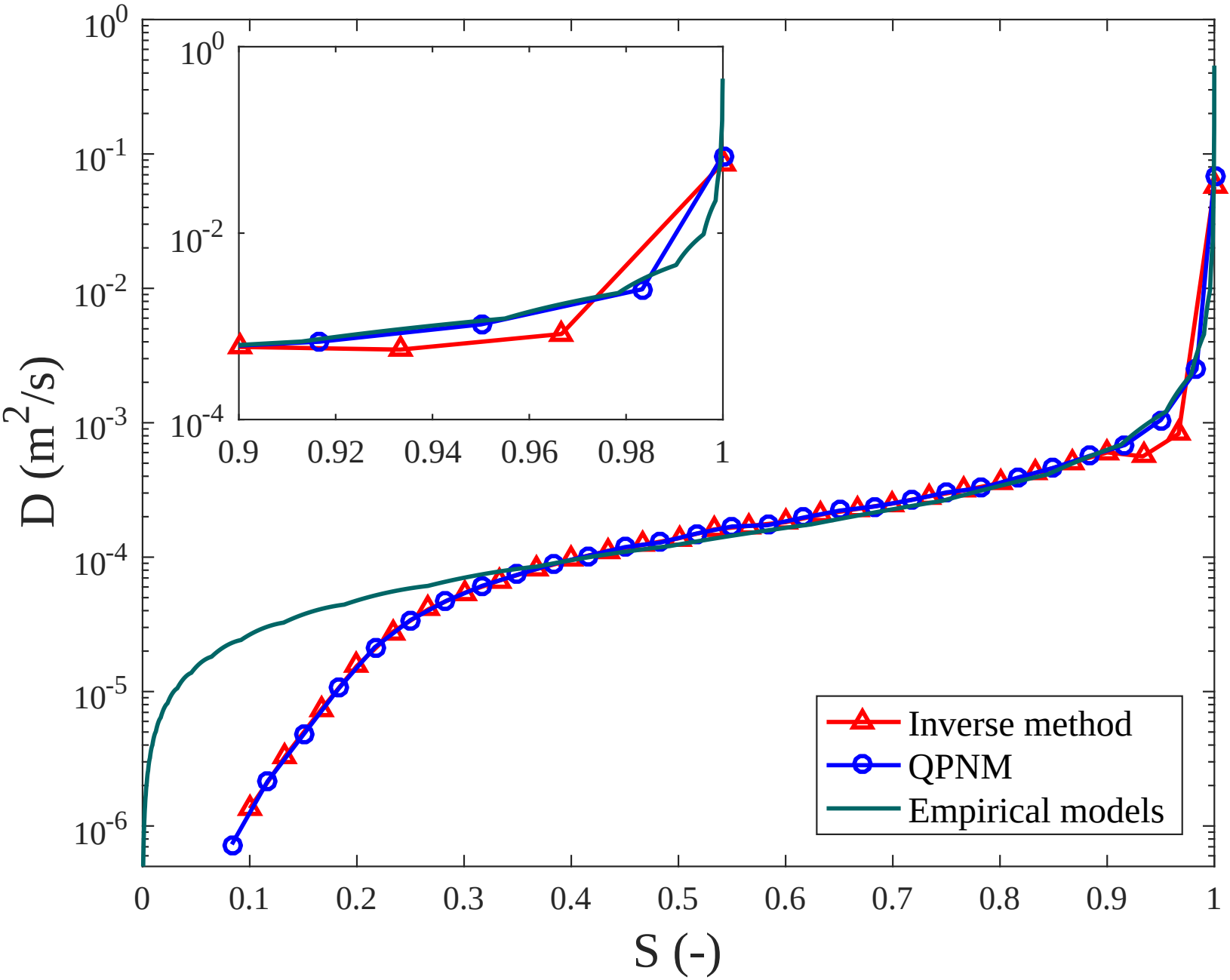

Figure 8

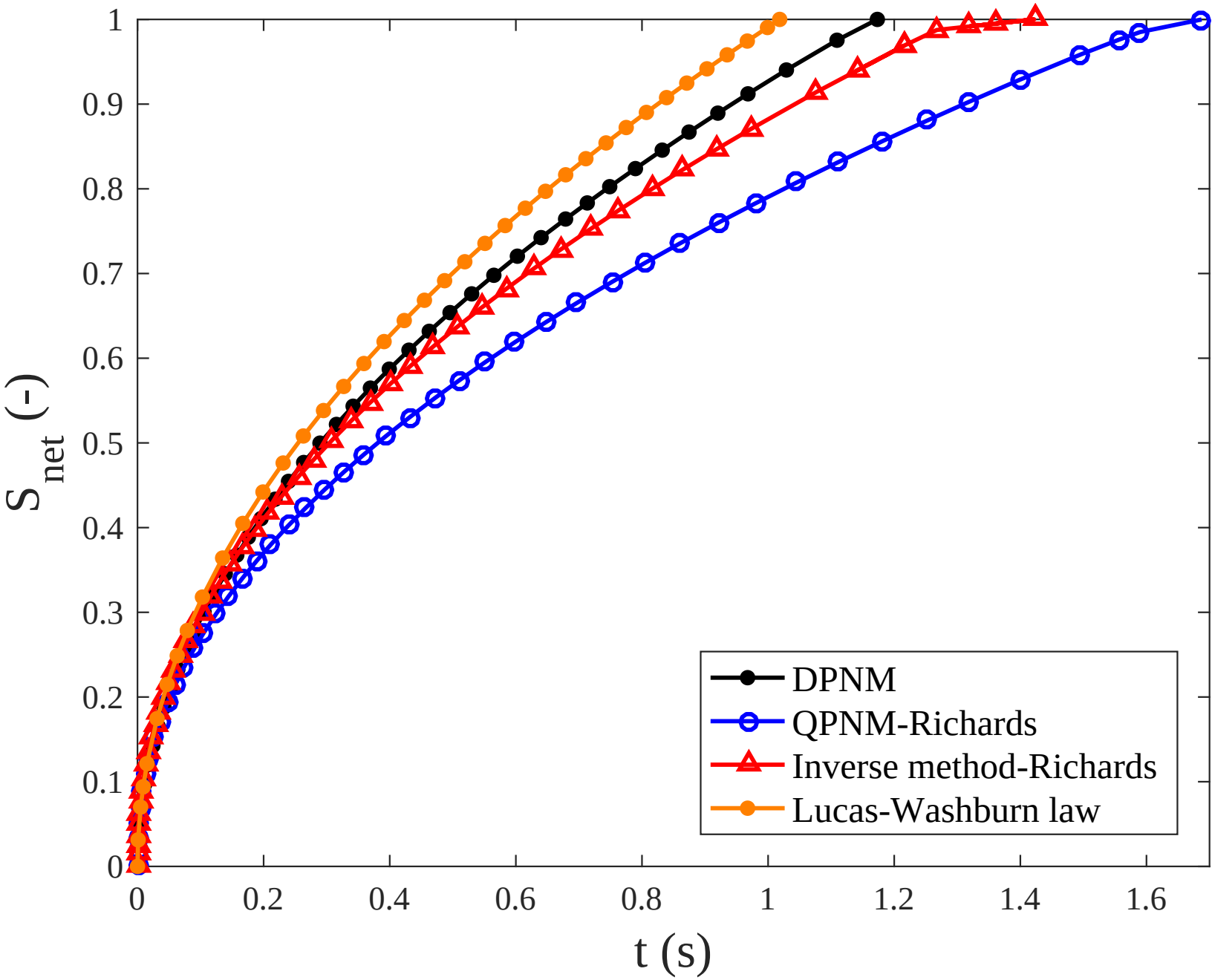
1
0.9
0.8
0.7
0.6
0.5
0.4
0.3
0.2
0.1
0
S net (-)
0
0.2
0.4
0.6
0.8
1
1.2
1.4
1.6
t (s)
DPNM
QPNM-Richards
Inverse method-Richards
Lucas-Washburn law

Figure 9

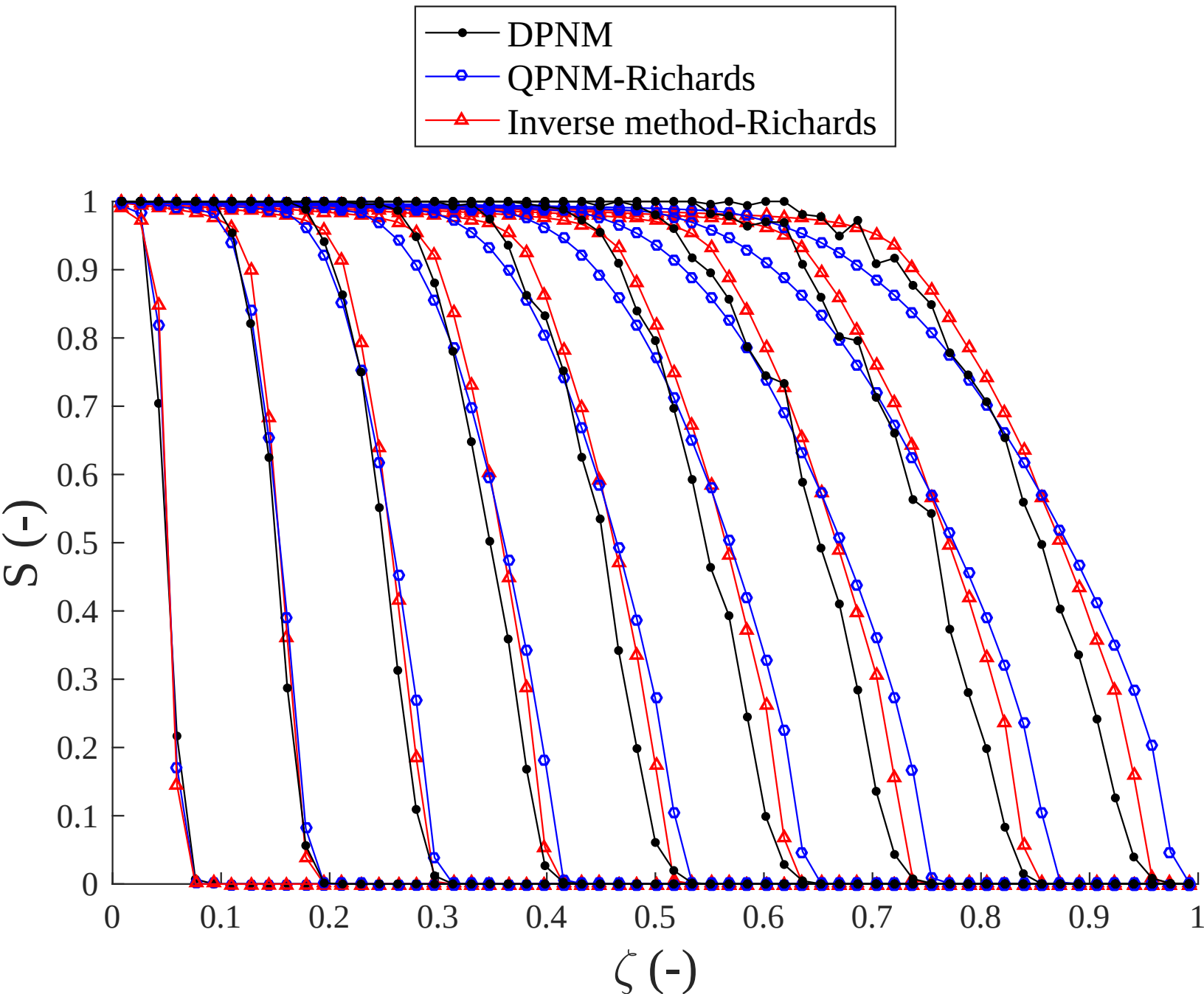
DPNM
QPNM-Richards
Inverse method-Richards
S (-)
ζ (-)
0
0.1
0.2
0.3
0.4
0.5
0.6
0.7
0.8
0.9
1

Figure 10

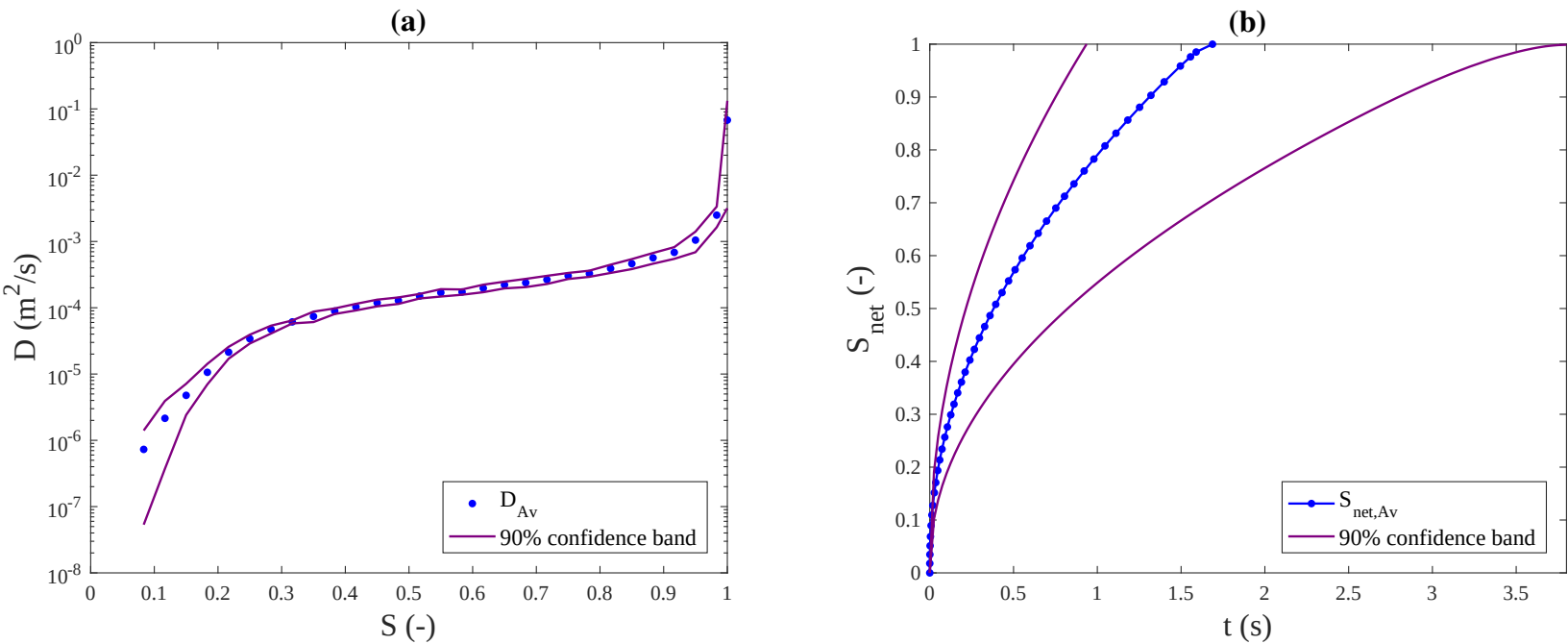
(a)
D (m²/s)
S (-)
D_Av
90% confidence band
(b)
S_net (-)
t (s)
S_net,Av
90% confidence band

Table1

Parameter	Value
Mean throat radius (μm)	250
Maximum throat radius (μm)	464.46
Minimum throat radius (μm)	54.22
Standard deviation of throat radii (%)	20%
Throat length (mm)	1
Coordination number (-)	6
Network size (nodes)	15×15×60
Air pressure (atm)	1
liquid inlet pressure	1
Dynamic viscosity of water (mPas)	0.89
Surface tension (N/m)	0.07197
Mass density of water (Kg/m^3)	996.93
Contact angle (°)	0
Porosity (-)	0.6946

Table 2

	Fitting parameters		Goodness of fit	
Parameter	n	$\alpha\ (1/\mathrm{Pa})$	R^2	RSS
Value	10.243	0.00189	0.995	0.13406

Table 3

	Fitting parameters	Goodness of fit	
Parameter	k	R^2	RSS
Value	1.853	0.997	0.08266

Table 4

Method	QPNM	Bundle of capillary model
Value (m^2)	1.8349×10^{-9}	1.7429×10^{-9}